Southern Hemisphere subtropical drying as a transient response to warming

Citation for published version:
Sniderman, JMK, Brown, JR, Woodhead, JD, King, AD, Gillett, NP, Tokarska, KB, Lorbacher, K, Hellstrom, J, Drysdale, RN & Meinshausen, M 2019, 'Southern Hemisphere subtropical drying as a transient response to warming', Nature Climate Change. https://doi.org/10.1038/s41558-019-0397-9

Digital Object Identifier (DOI):
10.1038/s41558-019-0397-9

Published In:
Nature Climate Change

Southern Hemisphere subtropical drying as a transient response to warming

Authors: J.M. Kale Sniderman[1]*, Josephine R. Brown[2], Jon D. Woodhead[1]*, Andrew D. King[1,3], Nathan P. Gillett[4], Katarzyna B. Tokarska[5,6], Katja Lorbacher[7], John Hellstrom[1], Russell N. Drysdale[8,9] and Malte Meinshausen[1,6,10]

Affiliations:

[1]School of Earth Sciences, University of Melbourne, Parkville, Victoria, 3010, Australia.

[2]Bureau of Meteorology, 700 Collins St, Docklands, Victoria, 3008, Australia.

[3]ARC Centre of Excellence for Climate Extremes, University of Melbourne, Parkville 3010, Victoria, Australia.

[4]Canadian Centre for Climate Modelling and Analysis, Environment and Climate Change Canada, University of Victoria, PO Box 1700, STN CSC, Victoria, British Columbia V8W 2Y2, Canada.

[5]School of Earth and Ocean Sciences, University of Victoria, 3800 Finnerty Road, Victoria, British Columbia V8W 3V6, Canada

[6]School of Geosciences, University of Edinburgh, The King's Buildings, Alexander Crum Brown Road, Edinburgh EH9 3FF, UK

[7]Australian-German Climate & Energy College, The University of Melbourne, Parkville 3010, Victoria, Australia

[8]School of Geography, University of Melbourne, Parkville, VIC 3010, Australia.

[9]Environnements, Dynamiques et Territoires de la Montagne, UMR CNRS, Université de Savoie-Mont Blanc, 73376 Le Bourget du Lac, France.

[10]Potsdam Institute for Climate Impact Research, Telegraphenberg, 14412 Potsdam, Germany

*Correspondence to: jdwood@unimelb.edu.au, kale.sniderman@unimelb.edu.au

Climate projections[1, 2, 3] and observations over recent decades[4, 5] indicate that precipitation in subtropical latitudes declines in response to anthropogenic warming, with significant implications for food production and population sustainability. However, this conclusion is

derived from emissions scenarios with rapidly increasing radiative forcing to the year 2100[1, 2], which may represent very different conditions from both past and future 'equilibrium' warmer climates. Here, we examine multi-century future climate simulations to demonstrate that in the Southern Hemisphere (SH) subtropical drying ceases soon after global temperature stabilises. Our results suggest that 21st century SH subtropical drying is not a feature of warm climates *per se*, but is primarily a response to rapidly rising forcing and global temperatures, as tropical sea-surface temperatures (SSTs) rise more than southern subtropical SSTs under transient warming. Subtropical drying may therefore be a temporary response to rapid warming: as greenhouse gas concentrations and global temperatures stabilise, SH subtropical regions may experience positive precipitation trends.

As Earth's climate warms in response to rising greenhouse gas (GHG) concentrations, average global precipitation is expected to increase (Supplementary Fig. 1), but zonally-averaged subtropical precipitation is projected to decrease[1, 6, 7]. Several mechanisms have been proposed for this decline, including thermodynamic processes in which wet regions get wetter and dry regions get drier[6]; and dynamic changes[7], such as the latitudinal expansion of the tropical overturning (Hadley) circulation[8] and poleward shifts in the westerlies[4, 9]. Recent studies have suggested a central role for the fast response to direct radiative forcing of CO_2[ref[10]], resulting in changes in land-sea temperature contrast and a decline in subtropical precipitation, predominantly over the ocean[11]. Subtropical drying may already be evident in the Southern Hemisphere, where recent decades have witnessed declining cool-season frontal precipitation, leading to drying over regions such as southern Australia[2, 4, 5]. Coupled Model Intercomparison Project Phase 5 (CMIP5)[12] projections under high emissions scenarios show a high level of consensus that this cool-season trend will continue until 2100 CE[1].

In contrast to this projected warmer and drier future, evidence from warm climates of the geologically recent past suggests that wetting, rather than drying, has been the equilibrium response of subtropical precipitation to warmer-than-present climate states. For example, during the Pliocene epoch (5.3-2.6 million years ago), global temperatures were ≥3°C warmer than pre-industrial and atmospheric CO_2 is estimated to have been ca. 400 ppm, while global land-sea configurations and continental topography were similar to today[13]. In response to warm Pliocene temperatures, subtropical regions of both hemispheres were generally wetter than today[14, 15, 16, 17]. Thus there is an apparent contradiction between a projected warm, dry future subtropics and its reconstructed warm, wet past[18, 19].

Most climate simulations have focused on the transient climates of the 21st century, with rapidly changing radiative forcing and temperatures that have few parallels in the geological record. Increased interest in the impacts of stabilising global mean temperature at a desired level[20, 21] raises the question of what a warmer than present-day, equilibrium climate state will look like, in contrast to better-studied, highly transient future climates. We therefore pose the question: are 21st century subtropical drying trends transient, or will the drier subtropics persist in an equilibrium or near-equilibrium warmer climate?

In order to address this question, we explore the evolution of subtropical precipitation under future, multi-century, warm-climate scenarios in which temperatures begin to stabilise following a projected rapid increase during most or all of the 21st century. Although most current-generation climate models do not adequately represent important 'slow' components of the climate system (e.g. ice sheets, dynamic vegetation) that equilibrate with forcing over centuries to millennia[22, 23], we refer to the period following stabilisation of radiative forcing in these simulations as a 'near-equilibrium' state, to distinguish it from the rapidly changing forcing and temperatures that are expected to characterise much of the current century. This is not to be confused with a full geological 'equilibrium' state achieved only after many centuries to millennia of changes in ice sheet extent, vegetation, and deep ocean warming[24, 25].

To evaluate precipitation responses to future near-equilibrium climates, we examined subtropical precipitation in scenarios in which GHG concentrations and temperatures stabilise during multi-century simulations. We examined subtropical precipitation in CMIP5 model runs under Representative Concentration Pathways 4.5 and 8.5, using their extensions to 2300 CE (ECPs 4.5 and 8.5)[26]. Both ECPs represent worlds with high atmospheric CO_2 (~2× and ~7× pre-industrial by 2300, respectively) but in ECP 4.5 atmospheric CO_2 concentrations stabilise by the year ~2080, while in ECP 8.5 stabilisation is not reached until the year ~2250, at much higher global temperatures (Supplementary Fig. 2). In addition, we examined an even longer simulation using CanESM1 extending to 3000 CE, based on a scenario of rapidly increasing atmospheric CO_2 concentrations (to ~2.7× pre-industrial) followed by complete cessation of emissions at 2100 [ref [27]] (Supplementary Fig. 3).

The Southern Hemisphere subtropical precipitation trends, averaged over all longitudes within the latitude range 25°S-35°S (Fig. 1), show that the 21st century decline occurs in the austral winter (represented by June through August precipitation, JJA), consistent with previous studies[1]. The JJA SH subtropical drying trend flattens, or reverses, soon after 2100 CE in ECP 4.5 and around 2200 CE in ECP 8.5 (Fig. 1). Thus SH subtropical precipitation reductions are greatest in JJA and in the 21st century, under both ECPs. Soon after the rate of warming declines (Supplementary Fig. 2), in both ECP 4.5 and ECP 8.5, JJA precipitation trends change from negative, to near zero or positive in several models in ECP4.5, and to positive in all models in ECP8.5 (Fig. 1).

Spatial patterns of the precipitation trends for ECP8.5 are shown in Fig. 2 (equivalent ECP4.5 trends are shown in Supplementary Fig. 4). In the 21st century, JJA SH subtropical precipitation trends are predominantly negative, especially in regions with high model agreement (indicated by stippling), including over both land and ocean. By the 23rd century, the JJA SH subtropics exhibits a pattern of weaker largely positive precipitation trends with some areas of high model agreement, again over both land and ocean. The ECP8.5 annual SH subtropical precipitation trend also changes from largely negative values in the 21st century to weaker positive trends in the 23rd century.

In order to explore the drivers of these reversals in the sign of precipitation change, we examined changes in the SH meridional temperature gradient (MTG), calculated as the difference between 0-10°S and 25-35°S zonal mean sea-surface temperatures (note, results are similar when different definitions of the MTG are used, see Methods), as the MTG influences the strength of the Hadley circulation, and hence the position and intensity of its descending subtropical branch[28, 29, 30]. We first consider the relationship of the MTG to JJA precipitation, since projected SH subtropical drying is most pronounced in the austral winter season. During the 21st century under transient warming, CMIP5 models generally show significantly decreasing JJA precipitation and a steepening MTG, under both ECP 4.5 and 8.5 (Fig. 3a,d). Under ECP 4.5, in the 22nd and 23rd centuries CMIP5 JJA precipitation and MTG trends are mostly indistinguishable from unforced variability (Methods). The CanESM1 simulation (Fig. 3g) follows a similar evolution from steepening MTG and declining JJA precipitation under transient 21st century warming, to weakly positive trends in JJA precipitation and negative MTG trends after and beyond 2100, as global temperatures stabilise. By comparison, under ECP 8.5, in which CO_2 and global temperature are still rising through the 22nd century (Supplementary Fig. 2), a transition to uniformly negative MTG trends and uniformly positive JJA precipitation trends (6 out of 9 models have significant trends) is deferred until the 23rd century (Fig. 3f), corresponding to the slowing of GHG increase and its complete stabilisation by 2250.

Thus MTG steepening appears to be closely linked to the rate of change of warming, since it shallows soon after CO_2 concentrations stabilise, around 2100 in ECP 4.5 and in the CanESM1 simulation, and by 2250 in ECP 8.5 (Supplementary Figs. 2 and 3). This shift to a shallowing MTG is generally associated with a recovery of JJA precipitation; the magnitude of this recovery (weak in ECP 4.5 and stronger in ECP 8.5) corresponds to the magnitude of warming. In summary, SH subtropical austral winter precipitation, in both CMIP5 models and CanESM1, seems to be closely linked to changing meridional gradients in SH SST warming. As the models approach global surface temperature equilibrium, warming is greater in the subtropics than the tropics and initially declining subtropical SH JJA precipitation trends reverse. These results are consistent with an earlier study based on a single model and using idealised experiments[29] that identified a reversal in SH subtropical precipitation trends in one region following a stabilisation of GHG concentrations and shifts in meridional temperature and pressure gradients.

In contrast to the JJA precipitation pattern of initial drying followed by a reversal, austral summer (DJF) precipitation trends, over the 2006-2300 CE interval, are overwhelmingly positive in ECP 8.5 (Figs. 3d-f). In ECP 4.5, the majority (10/16) of DJF precipitation trends are significantly positive, although there are two models with significantly negative trends and four with no significant trend, possibly reflecting intermodel differences in the importance of dynamic processes[7] in this lower-emissions scenario. Because they show little relationship to MTG trends (Fig. 3) but approximately scale with global temperature (Fig. 1), it seems likely that steady increases in DJF precipitation are either a thermodynamic response[7] to warming, or a dynamic response related to tropical, rather than mid-latitude circulation. In summary, model simulations indicate that, after initial transient winter drying, winter, summer and annual SH subtropical precipitation eventually increase with warming (Fig. 1, Supplementary Figs. 5 and 6).

Previous analyses[11] have suggested that the 21st century subtropical drying trend occurs predominantly over the ocean; we find that the models simulate stronger drying trends over ocean areas in the SH subtropics, but the proportionally small SH subtropical land areas also show 21st C JJA drying trends, and a reversal of this trend in the 22nd and 23rd centuries (Figure 2, Supplementary Fig. 7). Other studies[31] have suggested that the spatial pattern of precipitation change is driven by patterns of SST change as regions that warm least become drier, while regions that warm most become wetter. This is broadly consistent with our results, as the relatively weaker warming in the subtropics leads to a reduction in JJA subtropical precipitation in the transient part of the simulations, which reverses in the near-equilibrium part of the simulations. The relatively weaker warming in the SH subtropical ocean during transient warming may be driven by strengthened trade winds in that hemisphere[31, 32]. Several additional mechanisms have been proposed to explain trends in subtropical precipitation: changes in stratospheric ozone concentrations, and trends in the Hadley Cell extent and the Southern Annular Mode. Investigation of these mechanisms indicates that they are unable to explain the identified reversal in austral winter precipitation trends as global temperatures stabilise (see Methods).

Our results indicate that subtropical precipitation in coupled climate models responds within decades to a slowing in the rate of global warming, which in the multi-model mean leads to a change in sign of SH subtropical winter and annual precipitation trends. While previous studies[33] have assumed that precipitation changes at all latitudes scale approximately with global temperature, we find that winter SH subtropical drying may be a transient response that is later succeeded by positive precipitation trends, as the slowing rate of global temperature change allows southern extratropical SST warming to catch up with tropical warming[24, 27, 32]. While SH subtropical winter precipitation undergoes a reversal in trend, summer precipitation consistently increases with warming, potentially resulting in an overall increase in annual mean subtropical precipitation in a 'near-equilibrium' warmer world. We conclude that future subtropical precipitation changes beyond the traditional IPCC projection timeframe (to 2100) may not simply involve intensification of 21st century trends, but that cessation of subtropical drying may rapidly follow stabilisation of GHG concentrations. Reconstructions of subtropical precipitation during past warmer climate states suggest that wetting, rather than drying, is the long-term response of subtropical regions to warmer climates. If the long-term future response in these regions is also wetting, the apparent discrepancy between past and future subtropical precipitation under warm climates may be resolved as future climates move from a rapidly warming to a near-equilibrium state.

Figure legends

Figure 1 | Future precipitation projections. CMIP5 model time series of **a, b** global mean temperature, **c**, **d**, annual Southern Hemisphere (SH) meridional temperature gradient (SST 0-10°S – SST 25-35°S), and SH subtropical (25°S -35°S zonal mean) **e**, **f**, austral winter (JJA), **g**, **h**, austral summer (DJF) and **i, j,** annual (Ann) precipitation to 2300 CE under Extended Representative Concentration Pathway (ECP) 4.5 (**left**) and 8.5 (**right**), all expressed as anomalies relative to the 1986-2005 mean. Thick lines are multi-model mean and thin lines are individual models (ECP 4.5 has 16 models and ECP 8.5 has 9 models). All data is Loess-filtered.

Figure 2 | ECP8.5 Annual, DJF and JJA precipitation trends (mm/day/century) for the 21st, 22nd and 23rd centuries, 25°S-35°S subtropical band indicated**.** Stippling indicates 80% of models (8/9) agree on the sign of the trend. Spatial plots of ECP4.5 precipitation trends are shown in Supplementary Fig. 4.

Figure 3 | Relationship between the SH meridional temperature gradient (MTG) and SH subtropical precipitation. a-f, slopes of linear trends (K/century) of the MTG (difference between 0-10°S and 25°S-35°S zonal mean temperature) vs. slope of linear trends (mm/day/century) of subtropical seasonal precipitation (25-35°S zonal mean), for **a**,**d**, 21st century (2006-2100 CE), **b**,**e**, 22nd century (2101-2200 CE), and **c**,**f,** 23rd century (2201-2300 C), under scenarios ECP 4.5 (**a-c**, upper panels, n = 16) and ECP 8.5 (**d-f**, lower panels, n = 9). **g**,**h** for the CanESM1 simulation, showing 21st through 30th centuries (centuries labelled), with seasons **g**, JJA, and **h**, DJF, shown separately. **a-f**, for JJA, filled circles represent values that exceed two standard deviations of CMIP5 unforced control simulations (Methods, Supplementary Fig. 14); unfilled dots represent values indistinguishable from unforced control simulations. Double-headed arrows show the direction of wetting vs. drying, and shallowing vs. steepening of the MTG.

Correspondence and requests for materials should be addressed to J.M.K.S.

Acknowledgements

We thank Pandora Hope, Linden Ashcroft, Bertrand Timbal and Robert Colman for comments on versions of the manuscript, and Penny Whetton for discussions about this study. This research program was supported by Australian Research Council Grants DP0985214 (to JDW), DP130101829 (to JDW and RD), DE120102530 (to JMKS), FT130100801 (to JH), and DE180100638 (to ADK). We acknowledge the World Climate Research Programme's Working Group on Coupled Modelling, which is responsible for CMIP, and we thank the climate modelling groups (listed in Supplementary Table 1) for producing and making available their model output. For CMIP the U.S. Department of Energy's Program for Climate Model Diagnosis and Intercomparison provides coordinating support and led development of software infrastructure in partnership with the Global Organization for Earth System Science Portals.

Author contributions

J.M.K.S, J.R.B., J.D.W., J.H. and R.D. conceived of the project; J.R.B., J.M.K.S., J.D.W., K.L., M.M., N.P.G. and K.B.T. and A.D.K. analysed and interpreted the climate model data; J.M.K.S., J.R.B. and J.D.W. wrote the paper with contributions from the other authors.

References

1. Collins M, Knutti R, Arblaster J, Dufresne J-L, Fichefet T, Friedlingstein P, *et al.* Long-term Climate Change: Projections, Commitments and Irreversibility. In: Stocker TF, Qin D, Plattner G-K, Tignor M, Allen SK, Boschung J, *et al.* (eds). *Climate Change 2013: The Physical Science Basis. Contribution of Working Group I to the Fifth Assessment Report of the Intergovernmental Panel on Climate Change* Cambridge University Press: Cambridge, UK, 2013.

2. CSIRO and Bureau of Meteorology. *Climate Change in Australia. Information for Australia's Natural Resource Management Regions: Technical Report*. CSIRO and Bureau of Meteorology, Australia, 2015.

3. Tokarska KB, Gillett NP, Weaver AJ, Arora VK, Eby M. The climate response to five trillion tonnes of carbon. *Nature Climate Change* 2016, **6:** 851-855.

4. Cai W, Cowan T, Thatcher M. Rainfall reductions over Southern Hemisphere semi-arid regions: the role of subtropical dry zone expansion. *Scientific Reports* 2012, **2, article 702**.

5. Nguyen H, Lucas C, Evans E, Timbal B, Hanson L. Expansion of the Southern Hemisphere Hadley Cell in response to greenhouse gas forcing. *Journal of Climate* 2015, **28:** 8067-8077.

6. Held IM, Soden BJ. Robust Responses of the Hydrological Cycle to Global Warming. *Journal of Climate* 2006, **19:** 5686-5699.

7. Seager R, Naik N, Vecchi GA. Thermodynamic and dynamic mechanisms for large-scale changes in the hydrological cycle in response to global warming. *Journal of Climate* 2010, **23:** 4651-4668.

8. Seidel DJ, Fu Q, Randel WJ, Reichler TJ. Widening of the tropical belt in a changing climate. *Nature Geosci* 2008, **1**(1)**:** 21-24.

9. Scheff J, Frierson D. Twenty-First-Century multimodel subtropical precipitation declines are mostly midlatitude shifts. *Journal of Climate* 2012, **25:** 4330-4347.

10. Bony S, Bellon G, Klocke D, Sherwood S, Fermepin S, Denvil S. Robust direct effect of carbon dioxide on tropical circulation and regional precipitation. *Nature Geosci* 2013, **6**(6)**:** 447-451.

11. He J, Soden BJ. A re-examination of the projected subtropical precipitation decline. *Nature Clim Change* 2017, **7**(1)**:** 53-57.

12. Taylor KE, Stouffer RJ, Meehl GA. An Overview of CMIP5 and the Experiment Design. *Bulletin of the American Meteorological Society* 2012, **93**(4)**:** 485-498.

13. Haywood AM, Hill DJ, Dolan AM, Otto-Bliesner BL, Bragg F, Chan WL, *et al.* Large-scale features of Pliocene climate: results from the Pliocene Model Intercomparison Project. *Climate of the Past* 2013, **9**(1)**:** 191-209.

14. Salzmann U, Haywood AM, Lunt DJ, Valdes PJ, Hill DJ. A new global biome reconstruction and data-model comparison for the Middle Pliocene. *Global Ecology and Biogeography* 2008, **17**(3)**:** 432-447.

15. Sniderman JMK, Woodhead JD, Hellstrom J, Jordan GJ, Drysdale RN, Tyler JJ*, et al.* Pliocene reversal of late Neogene aridification. *Proceedings of the National Academy of Sciences* 2016, **113:** 1999-2004.

16. Amidon WH, Fisher GB, Burbank DW, Ciccioli PL, Alonso RN, Gorin AL*, et al.* Mio-Pliocene aridity in the south-central Andes associated with Southern Hemisphere cold periods. *Proceedings of the National Academy of Sciences* 2017, **114**(25)**:** 6474-6479.

17. Fauquette S, Suc JP, Guiot J, Diniz F, Feddi N, Zheng Z*, et al.* Climate and biomes in the West Mediterranean area during the Pliocene. *Palaeogeography Palaeoclimatology Palaeoecology* 1999, **152**(1-2)**:** 15-36.

18. Burls NJ, Fedorov AV. Wetter subtropics in a warmer world: Contrasting past and future hydrological cycles. *Proceedings of the National Academy of Science* 2017, **114:** 12888-12893.

19. Scheff J. Drought indices, drought impacts, CO2, and warming: a historical and geologic perspective. *Current Climate Change Reports* 2018, **4:** 202-209.

20. IPCC (ed). *Global warming of 1.5°C. An IPCC Special Report on the impacts of global warming of 1.5°C above pre-industrial levels and related global greenhouse gas emission pathways, in the context of strengthening the global response to the threat of climate change, sustainable development, and efforts to eradicate poverty*, 2018.

21. Zickfeld K, Eby M, Matthews HD, Weaver AJ. Setting cumulative emissions targets to reduce the risk of dangerous climate change. *Proceedings of the National Academy of Sciences* 2009, **106**(38)**:** 16129.

22. Rohling EJ, Sluijs A, Dijkstra H, Köhler P, van de Wal RSW, von der Heydt AS*, et al.* Making sense of palaeoclimate sensitivity. *Nature* 2012, **491**(7426)**:** 683-691.

23. Fischer H, Meissner KJ, Mix AC, Abram NJ, Austermann J, Brovkin V*, et al.* Palaeoclimate constraints on the impact of 2 °C anthropogenic warming and beyond. *Nature Geoscience* 2018, **11**(7)**:** 474-485.

24. Li C, von Storch JS, Marotzke J. Deep-ocean heat uptake and equilibrium climate response. *Climate Dynamics* 2013, **40:** 1071-1086.

25. Frölicher TL, Paynter DJ. Extending the relationship between global warming and cumulative carbon emissions to multi-millennial timescales. *Environmental Research Letters* 2015, **10**(7)**:** 075002.

26. Meinshausen M, Smith SJ, Calvin K, Daniel JS, Kainuma MLT, Lamarque JF*, et al.* The RCP greenhouse gas concentrations and their extensions from 1765 to 2300. *Climatic Change* 2011, **109**(1-2)**:** 213-241.

27. Gillett NP, Arora VK, Zickfeld K, Marshall SJ, Merryfield WJ. Ongoing climate change following a complete cessation of carbon dioxide emissions. *Nature Geoscience* 2011, **4**(2)**:** 83-87.

28. Kushner PJ, Held IM, Delworth TL. Southern hemisphere Atmospheric Circulation Response to Global Warming. *Journal of Climate* 2001, **14:** 2238-2249.

29. Cai WJ, Whetton PH, Karoly DJ. The Response of the Antarctic Oscillation to increasing and stabilized amospheric CO2. *Journal of Climate* 2003, **16:** 1525-1538.

30. Seo K-H, Frierson DMW, Son J-H. A mechanism for future changes in Hadley circulation strength in CMIP5 climate change simulations. *Geophysical Research Letters* 2014, **41**(14)**:** 5251-5258.

31. Xie S-P, Clara D, Vecchi GAV, Ma J, Teng H, Wittenberg AT. Global Warming Pattern Formation: Sea Surface Temperature and Rainfall. *Journal of Climate* 2010, **23**(4)**:** 966-986.

32. Long S-M, Xie S-P, Zheng X-T, Liu Q. Fast and Slow Responses to Global Warming: Sea Surface Temperature and Precipitation Patterns. *Journal of Climate* 2014, **27**(1)**:** 285-299.

33. Solomon S, Plattner G-K, Knutti R, Friedlingstein P. Irreversible climate change due to carbon dioxide emissions. *Proceedings of the National Academy of Sciences* 2009, **106**(6)**:** 1704-1709.

Methods

Models and variables used. We examined global temperature and SH subtropical precipitation trends to 2300 CE under two Extended Concentration Pathway (ECP) scenarios, ECP 4.5 and ECP 8.5[12, 26]. We examined results from nine models for ECP 8.5, and sixteen models for ECP 4.5 (Supplementary Table 1). ECP 4.5 and ECP 8.5 represent continuations beyond 2100 of RCP 4.5 and 8.5 scenarios, respectively, using idealised emission trajectories that lead to stabilisation of greenhouse gas forcing at c. 4.5 W m^{-2} by c. 2080 CE under ECP 4.5 (corresponding to c. 550 ppm CO_2), and at c. 12.5 W m^{-2} by 2250 CE, under ECP 8.5 (corresponding to c. 1900 ppm CO_2)[26] (Supplementary Fig. 1). To examine whether ECP trends continued beyond 2300 CE, we examined global temperature and SH subtropical precipitation in an idealised simulation extending to 3000 CE using CanESM1, in which CO_2 increases rapidly (to ~2.7× pre-industrial) followed by complete cessation of emissions at 2100 CE[27]. Further details of the model and experimental design for the CanESM1 simulation is provided in reference [[27]].

Monthly fields of global surface temperature (Ts for CMIP5, TAS for CanESM1), zonally averaged SH tropical and subtropical temperature (annual zonal mean sea surface temperature, SST, in two latitudinal bands, 0-10°S, and 25-35°S), and SH subtropical precipitation (defined as the average for all grid points in a zonal band, 25°S-35°S, both for the entire zonal band, and for ocean and land surfaces separately – see Supplementary Fig. 7) were obtained for each CMIP5 model over the period 2006-2300 CE, and for the CanESM1 simulation over the period 2006-3000 CE. The corresponding historical simulations (1986-2005) were obtained from each model to provide a reference period, following IPCC AR5 convention (e.g. ref [1]). The annual and seasonal mean SH subtropical precipitation for DJF and JJA was calculated for each year. The yearly anomaly of Annual, DJF and JJA SH subtropical precipitation for each of the nine ECP 8.5 simulations, 16 ECP 4.5 simulations, and the CanESM1 simulation was calculated for each year of the simulation relative to the historical reference period. The anomalies are plotted in Fig. 1 using robust Loess smoothing[34] to remove inter-annual to inter-decadal scale variability.

Our definition of the SH subtropics as a zonal band extending between 25-35°S, representing a commonly used definition of the subtropics[35]. Analyses with alternative definitions of this band (20-40°S, 28-38°S) suggested that the precipitation response identified here is not sensitive to the definition of these equatorward or poleward boundaries (Supplementary Fig. 8). The exact location of the subtropical boundaries will vary from model to model, and may also shift over time. We choose a zonal band that corresponds to a shared region of coherent climate response, and excludes the latitudes where the boundary between subtropical drying and midlatitude wetting occurs (see Supplementary Figs. 5, 6).

Calculation of meridional temperature gradient. To examine the relationship over time between SH subtropical precipitation and the SH meridional temperature gradient (MTG), we calculated a metric of the annual mean SH MTG as the difference between 0-10°S and 25°S-35°S zonal mean sea surface temperature (SST) (Supplementary Fig. 9). The chosen low and high latitude boundaries are consistent with a range of studies that evaluate observed and future changes in the strength and poleward extent of the Hadley Cell, which largely governs moisture transport between the tropics and subtropics. We conducted sensitivity tests (not shown) with alternative definitions of the SH MTG (viz. 10°N-10°S minus 10°-30°S; 20°N-20°S minus 20°S-40S; and 0-10°S minus 40°S-60°S), consistent with various definitions used in recent studies[30, 36, 37]. These analyses indicated that our results are not sensitive to our choice among these definitions of equatorial and subtropical/mid-latitude bands. We divided each CMIP5 time series and the CanESM1 time series into three ~equivalent windows defined by the years 2006-2100, 2101-2200, and 2201-2300 CE. For the CanESM1 time series we also defined a fourth window between 2301-3000 CE. Within each time window we calculated linear trends of the MTG and of SH subtropical precipitation for JJA and DJF.

Southern Annular Mode and Hadley Cell extent as possible drivers. The role of changes in the latitude of the southern margin of the Hadley Cell was investigated, as some studies have suggested that subtropical precipitation changes may be driven by a poleward expansion of the

Hadley circulation (e.g. ref[38]). A related driver of subtropical precipitation change is the Southern Annular Mode (SAM), a mode of variability associated with the poleward shift of the mid-latitude westerlies in its positive (high SAM) phase. In the current climate, a high SAM results in increased SH subtropical rainfall in summer (and also spring and autumn) but reduced rainfall in winter[39]. Future projections to 2100 CE show an increased SAM in all seasons in response to increased greenhouse gases[40]. This positive SAM trend is expected to result in increased summer rainfall but reduced winter rainfall in the SH subtropics[41]. In addition, future projections show that the Hadley Cell will continue to expand poleward with increasing greenhouse gases (e.g. refs [1, 5, 42]). We investigated whether either SAM or Hadley Cell extent changes can explain the reversal in SH subtropical winter rainfall trends as global temperatures stabilise.

The SAM index is defined as the difference in the normalized zonally averaged sea level pressure between 40°S and 65°S (e.g. ref [43]). The SAM index was calculated for each model under ECP4.5 and ECP8.5 for DJF, JJA and Annual (Supplementary Fig. 10) and seasonal SAM trends calculated for the 21st, 22nd and 23rd centuries (Supplementary Fig. 11). Under ECP4.5, SAM trends are generally positive during the 21st century in all seasons, then SAM anomalies remain positive and stable in the 22nd and 23rd centuries (Supplementary Figs. 10 and 11). Under ECP8.5, SAM values increase most strongly in the 21st and 22nd centuries in both seasons and stabilise at a higher positive value during the 23rd century (Supplementary Figs. 10 and 11). Positive SAM values are consistent with increasing SH subtropical rainfall in austral summer and decreasing SH subtropical rainfall in austral winter in the transient parts of the ECP simulations[39, 41], but do not explain the reversal of winter rainfall trends following stabilisation of temperatures, as there is no clear reversal of SAM trends in any season.

The Hadley Cell edge is calculated from the latitude where the zonal mean meridional mass streamfunction is zero at 500 hPa (e.g. ref [44]). The latitude of the southern edge of the Hadley Cell was calculated for each model under ECP4.5 and ECP8.5 for DJF, JJA and Annual (Supplementary Fig. 12) and seasonal SAM trends calculated for the 21st, 22nd and 23rd centuries (Supplementary

Fig. 13). Similar to SAM, there is a clear southward displacement of the Hadley Cell edge in all seasons, with the latitude of the Hadley Cell edge stabilising around 2100 under ECP4.5 and around 2200 under ECP8.5 (Supplementary Fig. 12). The trends in Hadley Cell edge latitude are southward (negative) under transient climate (ECP4.5 21st century and ECP8.5 21st and 22nd centuries) and then near zero following stabilisation of global temperatures (Supplementary Fig. 13). There is no reversal of the trend in Hadley Cell edge latitude, so we conclude that changes in the southward extent of the Hadley Cell do not drive the reversal in SH subtropical winter rainfall trends.

Ozone recovery. Stratospheric ozone depletion in the historical period has been linked to increases in austral summer precipitation in the SH subtropics due to a poleward shift of the extratropical westerly jet[45]. The recovery of stratospheric ozone in the 21st century would therefore favour reduced austral summer precipitation, but the absence of such a summer drying trend in projections (including ECP4.5 and ECP8.5, see Fig. 1) indicates that GHG increases dominate the response (e.g. refs [40, 46, 47]). In addition, changes in stratospheric ozone concentrations are prescribed to return to pre-industrial levels by 2050 CE (ref [46]) therefore they cannot explain the reversal of JJA precipitation trends in ECP4.5 around 2080 and in ECP8.5 around 2200.

Comparison with control runs. In order to evaluate whether the observed linear trends of the SH MTG, and of SH subtropical JJA and DJF precipitation are significantly different from those expected under unforced variability, we obtained control runs for the 16 CMIP5 models that ran extended RCP simulations[12]. We used these control runs differently for JJA and DJF precipitation trends, for the following reasons. For JJA, 21st through 23rd century precipitation trends clearly show a reversal in sign which we have shown is closely linked to changes in the MTG (Fig. 3). Because our goal was to evaluate the significance of future bivariate MTG vs JJA precipitation change, we divided the control runs into 94 unique 100-year intervals, from which we extracted linear trends of the MTG and JJA precipitation. We standardised the 94 control run MTG and JJA precipitation data sets, then converted each standardised MTG slope vs. standardised JJA precipitation slope pair into its radial distance from the origin, using Pythagoras' theorem. We then standardised our 21st to 23rd century MTG and JJA precipitation trends with respect to the mean and standard deviation of the 94 control run MTG and JJA precipitation trends, respectively, before converting these standardised 21st to 23rd century trends to radial distances from the origin. Where the standardised radial distances of the 21st to 23rd century MTG vs JJA precipitation trend slopes are <2 standard deviations from the origin, measured in standardised units of the corresponding control runs' slopes, we interpret them as trends that might occur solely due to unforced variability; where their values are ≥ 2 standard deviations, we interpret them as unlikely to occur in the absence of increased GHG forcing (Supplementary Fig. 14).

For DJF, 21st through 23rd century precipitation trends show no change of sign, but, particularly in ECP 8.5, are consistently positive (Fig. 3), and do not have a strong relationship with the MTG. Therefore, we evaluated the significance of the DJF precipitation trends over the entire 2006 to 2300 interval, and employed a univariate approach. To evaluate the significance of these trends, we divided the control runs into 22 unique 295-year intervals, from which we extracted linear trends of DJF precipitation, and calculated their 2.5 and 97.5 percentiles (ca. –2 and + 2 standard deviations). Where the 2006-2300 DJF precipitation trends are ≤ -2 or $\geq +2$ standard deviations of the control DJF precipitation trends, we interpret them as unlikely to occur in the absence of increased GHG forcing (Supplementary Fig. 15).

Comparison with the full set of RCP simulations. Because only a subset of CMIP5 models (the "ECP models") undertook the extended simulations to 2300 CE (16 for ECP 4.5, nine for ECP 8.5), we evaluated the possibility that the ECP subset is a biased sample of the full set of CMIP5 models, by comparing the performance of the ECP models during the 21st century, with the full set of available CMIP5 models that solely undertook 21st century runs (the "RCP models"). We compared their performance using Student's T-tests, which indicated that mean 21st century trends of JJA and DJF precipitation and of the MTG in the ECP models are indistinguishable from those of the RCP models (Supplementary Fig. 16). We thus concluded that the ECP subset is broadly representative of the full set of CMIP5 models.

Data Availability

The authors declare that the data supporting the findings of this study are available within the article and its supplementary information files. The CMIP5 model data used in this study are available in public repositories, for example at https://esgf-node.llnl.gov/projects/esgf-llnl/. The model data used here were stored on the Australian node of the Earth System Grid (the National Computational Infrastructure). Data associated with the CanESM1 simulation used in this study is available at http://crd-data-donnees-rdc.ec.gc.ca/CCCMA/CanESM1_zero_emission.

Methods References

34. Cleveland WS, Devlin SJ. Locally Weighted Regression: An Approach to Regression Analysis by Local Fitting. *Journal of the American Statistical Association* 1988, **83:** 596-610.

35. American Meteorological Society. Subtropics. *Glossary of Meteorolog*y [Available online at http://glossary.ametsoc.org/wiki/"subtropics"]. 2018.

36. Adam O, Schneider T, Harnik N. Role of Changes in Mean Temperatures versus Temperature Gradients in the Recent Widening of the Hadley Circulation. *Journal of Climate* 2014, **27**(19)**:** 7450-7461.

37. D'Agostino R, Lionello P, Adam O, Schneider T. Factors controlling Hadley circulation changes from the Last Glacial Maximum to the end of the 21st century. *Geophysical Research Letters* 2017, **44**(16)**:** 8585-8591.

38. Scheff J, Frierson D. Robust future precipitation declines in the CMIP5 largely reflect the poleward expansion of model subtropical dry zones *Geophysical Research Letters* 2012(39)**:** doi:10.1029/2012GL052910

39. Hendon HH, Lim E-P, Nguyen H. Seasonal Variations of Subtropical Precipitation Associated with the Southern Annular Mode. *Journal of Climate* 2014, **27**(9)**:** 3446-3460.

40. Gillett NP, Fyfe JC. Annular mode changes in the CMIP5 simulations. *Geophysical Research Letters* 2013, **40**(6)**:** 1189-1193.

41. Lim E-P, Hendon HH, Arblaster JM, Delage F, Nguyen H, Min S-K*, et al.* The impact of the Southern Annular Mode on future changes in Southern Hemisphere rainfall. *Geophysical Research Letters* 2016, **43:** 7160-7167.

42. Lucas C, Timbal B, Nguyen H. The expanding tropics: a critical assessment of the observational and modeling studies. *Wiley Interdisciplinary Reviews: Climate Change* 2014, **5**(1)**:** 89-112.

43. Gong D, Wang S. Definition of Antarctic Oscillation index. *Geophysical Research Letters* 1999, **26**(4)**:** 459-462.

44. Solomon A, Polvani LM, Waugh DW, Davis SM. Contrasting upper and lower atmospheric metrics of tropical expansion in the Southern Hemisphere. *Geophysical Research Letters* 2016, **43**(19)**:** 10,496-410,503.

45. Kang SM, Polvani LM, Fyfe JC, Sigmond M. Impact of Polar Ozone Depletion on Subtropical Precipitation. *Science* 2011, **332**(6032)**:** 951-954.

46. Arblaster JM, Meehl GA. Contributions of external forcings to Southern Annular Mode trends. *Journal of Climate* 2006, **19**(12)**:** 2896-2905.

47. Arblaster JM, Meehl GA, Karoly DJ. Future climate change in the Southern Hemisphere: Competing effects of ozone and greenhouse gases. *Geophysical Research Letters* 2011, **38**(2)**:** L02701.

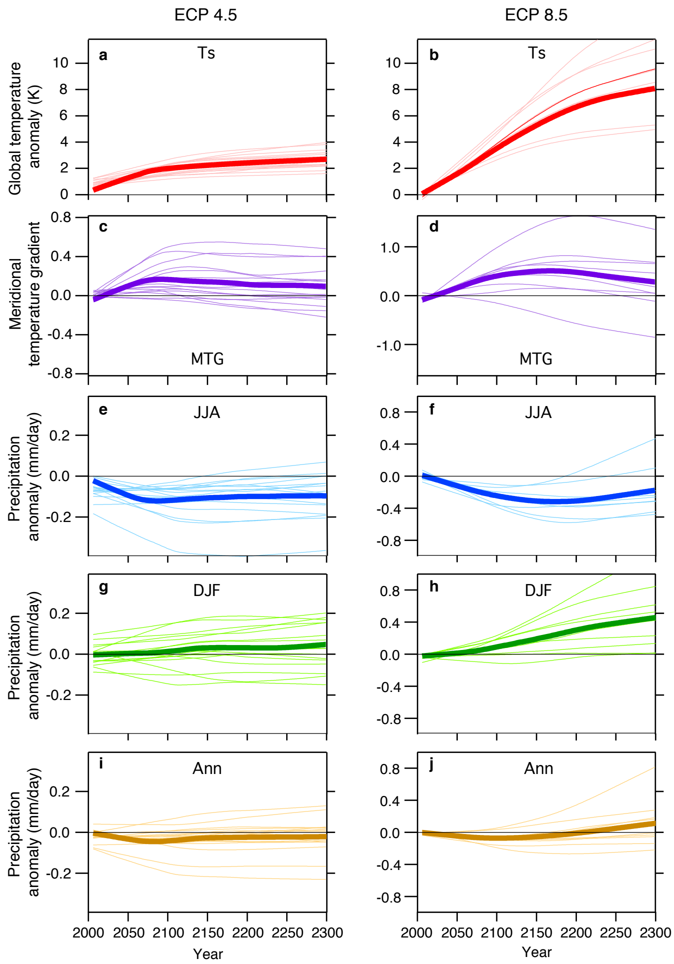

ECP 4.5
ECP 8.5
a
Ts
b
Ts
Global temperature anomaly (K)
c
MTG
d
MTG
Meridional temperature gradient
e
JJA
f
JJA
Precipitation anomaly (mm/day)
g
DJF
h
DJF
Precipitation anomaly (mm/day)
i
Ann
j
Ann
Precipitation anomaly (mm/day)
Year
Year

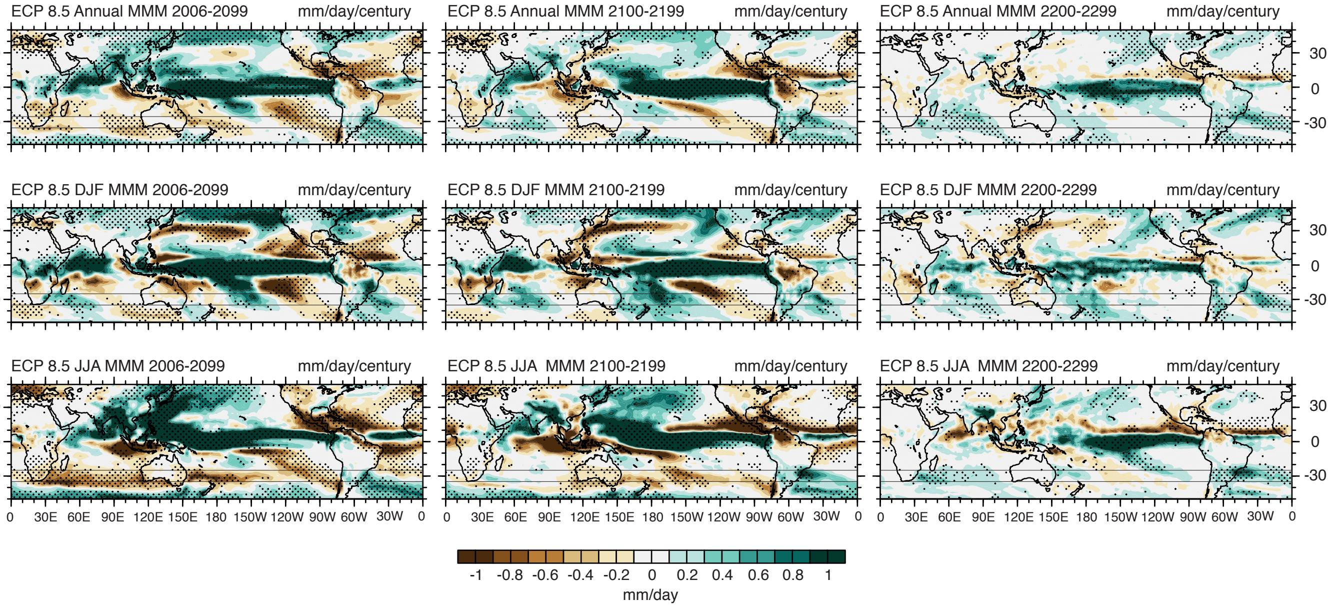
ECP 8.5 Annual MMM 2006-2099
mm/day/century
ECP 8.5 Annual MMM 2100-2199
mm/day/century
ECP 8.5 Annual MMM 2200-2299
mm/day/century
ECP 8.5 DJF MMM 2006-2099
mm/day/century
ECP 8.5 DJF MMM 2100-2199
mm/day/century
ECP 8.5 DJF MMM 2200-2299
mm/day/century
ECP 8.5 JJA MMM 2006-2099
mm/day/century
ECP 8.5 JJA MMM 2100-2199
mm/day/century
ECP 8.5 JJA MMM 2200-2299
mm/day/century
30
0
-30
0
30E
60E
90E
120E
150E
180
150W
120W
90W
60W
30W
0
-1
-0.8
-0.6
-0.4
-0.2
0
0.2
0.4
0.6
0.8
1
mm/day

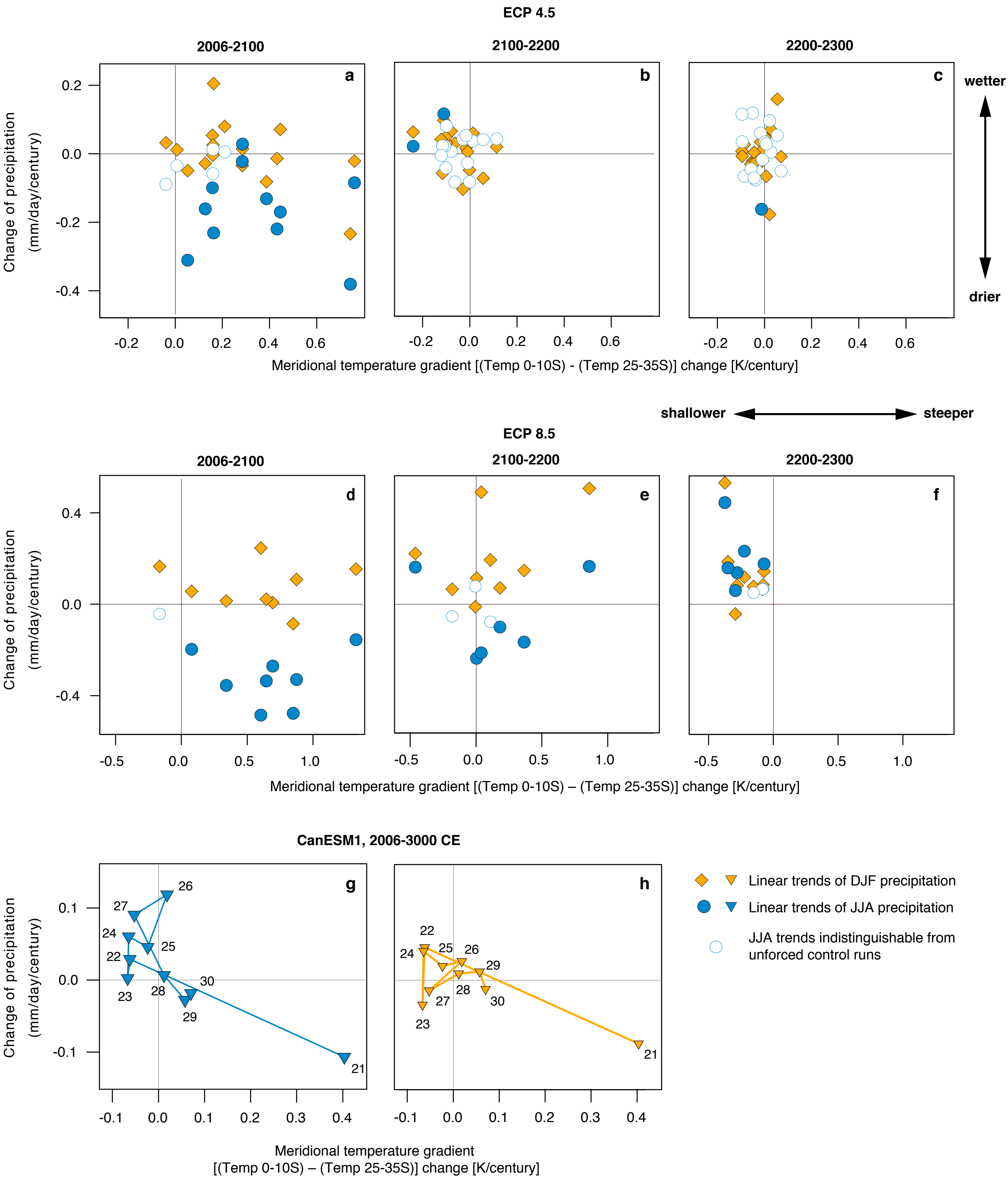
ECP 4.5
2006-2100
2100-2200
2200-2300
a
b
c
wetter
drier
Change of precipitation
(mm/day/century)
0.2
0.0
-0.2
-0.4
-0.2
0.0
0.2
0.4
0.6
Meridional temperature gradient [(Temp 0-10S) - (Temp 25-35S)] change [K/century]
shallower
steeper
ECP 8.5
2006-2100
2100-2200
2200-2300
d
e
f
0.4
0.0
-0.4
-0.5
0.0
0.5
1.0
Meridional temperature gradient [(Temp 0-10S) – (Temp 25-35S)] change [K/century]
CanESM1, 2006-3000 CE
g
h
0.1
0.0
-0.1
-0.1
0.0
0.1
0.2
0.3
0.4
21
22
23
24
25
26
27
28
29
30
Linear trends of DJF precipitation
Linear trends of JJA precipitation
JJA trends indistinguishable from
unforced control runs
Meridional temperature gradient
[(Temp 0-10S) – (Temp 25-35S)] change [K/century]